Synthesis of SnO_2 and ZnO Colloidal Nanocrystals from the Decomposition of Tin(II) 2-Ethylhexanoate and Zinc(II) 2-Ethylhexanoate

Mauro Epifani,*,† Jordi Arbiol,‡ Raül Díaz,‡ Mariano J. Perálvarez,‡ Pietro Siciliano,† and Joan R. Morante‡

Consiglio Nazionale delle Ricerche, Istituto per la Microelettronica ed i Microsistemi, CNR-IMM, Sezione di Lecce, via Arnesano, 73100 Lecce, Italy, and Departament d'Electrònica, Universitat de Barcelona, C. Martí i Franqués 1, 08028 Barcelona, Spain

Received July 26, 2005. Revised Manuscript Received October 10, 2005

We report for the first time the nonhydrolytic synthesis of soluble SnO_2 nanocrystals, by the decomposition at temperatures between 230 and 250 °C of tin(II) 2-ethylhexanoate in diphenyl ether and in the presence of amines as surface capping agents. X-ray diffraction (XRD) and high-resolution transmission electron microscopy (HRTEM) studies showed that highly crystalline nanoparticles were obtained with a mean size ranging from about 3 to about 3.5 nm, depending on the length of the alkyl chain of the amine. The use of metal 2-ethylhexanoate in the synthesis of oxide nanocrystals was generalized by preparing ZnO nanocrystals from the decomposition under similar conditions of zinc(II) 2-ethylhexanoate. In this case, soluble nanocrystals with a size ranging from about 5 to 8 nm were obtained. It is shown that the decomposition path of the precursor depends on the specific metal, and may result in the sudden formation of pyrolized products instead of soluble nanocrystals. The optical properties of capped SnO_2 nanocrystals are reported for the first time and are characterized by only a blue luminescence, while for the ZnO colloids the photoluminescence spectra are characterized by the typical band-edge and surface defects emission bands, but in these samples the latter band is unusually much weaker than the former.

1. Introduction

Following the extensive development of the synthesis of nanometric colloidal chalcogenide nanocrystals,[1] in particular as concerns II−VI systems, increasing attention has been devoted very recently to the preparation of oxide colloids. The existing synthetic routes generally rely on different principles with respect to the II−VI or III−V systems, and while, to the best of our knowledge, direct reaction between oxygen and an organometallic precursor has been reported only in one case,[2] the general emerging approaches to capped oxide colloids consist of the hydrolytic[3] or nonhydrolytic[4] sol−gel processing of metal halides or alkoxides or of the decomposition of oxygen-rich precursors, eventually already containing the metal−oxygen bond. Examples of the latter method display the use of metal cupferronates,[5] acetylacetonates,[6] acetates,[7] fatty acid salts,[8] and organometallics.[9] A different method is based on the in situ oxidation of metal nanoparticles.[10] In this rapidly developing field, the investigation of different precursors is then of remarkable interest, from a fundamental perspective and eventually for providing advantageous features with respect to the already used

* Corresponding author. E-mail: mauro.epifani@le.imm.cnr.it.
† CNR-IMM.
‡ Universitat de Barcelona.

(1) Murray, C. B.; Kagan, C. R.; Bawendi, M. G. *Annu. Rev. Mater. Sci.* **2000**, *30*, 545.
(2) Shim, M.; Guyot-Sionnest, P. *J. Am. Chem. Soc.* **2001**, *123*, 11651−11654.
(3) (a) O'Brien, S.; Brus, L.; Murray, C. B. *J. Am. Chem. Soc.* **2001**, *123*, 12085−12086. (b) Cozzoli, P. D.; Kornowski, A.; Weller, H. *J. Am. Chem. Soc.* **2003**, *125*, 14539−14548.
(4) (a) Trentler, T. J.; Denler, T. E.; Bertone, J. F.; Agrawal, A.; Colvin, V. L. *J. Am. Chem. Soc.* **1999**, *121*, 1613−1614. (b) Joo, J.; Yu, T.; Kim, Y. W.; Park, H. M.; Wu, F.; Zhang, J. Z.; Hyeon, T. *J. Am. Chem. Soc.* **2003**, *125*, 6553−6557.
(5) (a) Rockenberger, J.; Scher, E. C.; Alivisatos, A. P. *J. Am. Chem. Soc.* **1999**, *121*, 11595−11596. (b) Thimmaiah, S.; Rajamathi, M.; Singh, N.; Bera, P.; Meldrum, F.; Chandrasekhar, N.; Seshadri, R. *J. Mater. Chem.* **2001**, *11*, 3215−3221. (c) Ghosh, M.; Sampathkumaran, E. V.; Rao, C. N. R. *Chem. Mater.* **2005**, *17*, 2348−2352.
(6) (a) Sun, S.; Zeng, H. *J. Am. Chem. Soc.* **2002**, *124*, 8204−8205. (b) Seo, W. S.; Jo, H. H.; Lee, K.; Park, J. T. *Adv. Mater.* **2003**, *15*, 795−797.
(7) (a) Cozzoli, P. D.; Curri, M. L.; Agostiano, A.; Leo, G.; Lomascolo, M. *J. Phys. Chem B.* **2003**, *107*, 4756−4762. (b) Yin, M.; O'Brien, S. *J. Am. Chem. Soc.* **2003**, *125*, 10180−10181. (c) Yin, M.; Gu, Y.; Kuskovsky, Y. L.; Andelman, T.; Zhu, Y.; Neumark, G. F.; O'Brien, S. *J. Am. Chem. Soc.* **2004**, *126*, 6206−6207. (d) Joo, J.; Kwon, S. G.; Yu, J. H.; Hyeon, T. *Adv. Mater.* **2005**, *17*, 1873−1877. (e) Andelman, T.; Gong, Y.; Polking, M.; Yin, M.; Kuskovsky, Y.; Neumark, G.; O'Brien, S. *J. Phys. Chem. B* **2005**, *109*, 14314−14318. (f) Liu, Q.; Lu, W.; Ma, A.; Tang, J.; Lin, J.; Fang, J. *J. Am. Chem. Soc.* **2005**, *127*, 5276−5277.
(8) (a) Jana, N. R.; Chen, Y.; Peng, X. *Chem. Mater.* **2004**, *16*, 3931−3935. (b) Park, J.; An, K.; Hwang, Y.; Park, J.-G.; Noh, H.-J.; Kim, J.-Y.; Park, J.-H.; Hwang, N.-M.; Hyeon, T. *Nat. Mater.* **2004**, *3*, 891. (c) Choi, S.-H.; Kim, E.-G.; Park, J.; An, K.; Lee, N.; Kim, S. C.; Hyeon, T. *J. Phys. Chem. B* **2005**, *109*, 14792−14794. (d) Chen, Y.; Kim, M.; Lian, G.; Johnson, M. B.; Peng, X. *J. Am. Chem. Soc.* **2005**, *127*, 13331−13337.
(9) (a) Cheon, J.; Kang, N. J.; Lee, S. M.; Lee, J. H.; Joon, J. H.; Oh, S. J. *J. Am. Chem. Soc.* **2004**, *126*, 1950−1951. (b) Monge, M.; Kahn, M. L.; Maisonnat, A.; Chaudret, B. *Angew. Chem., Int. Ed.* **2003**, *115*, 5479−5482. (c) Kahn, M. L.; Monge, M.; Colliere, V.; Senocq, F.; Maisonnat, A.; Chaudret, B. *Adv. Funct. Mater.* **2005**, *15*, 458−468.
(10) (a) Hyeon, T.; Lee S. S.; Park, J.; Chung, Y.; Na, H. B. *J. Am. Chem. Soc.* **2001**, *123*, 12798−12801. (b) Cozzoli, P. D.; Kornowski, A.; Weller, H *J. Phys. Chem. B.* **2005**, *109*, 2638−2644.

10.1021/cm051642u CCC: $30.25
Published on Web 11/12/2005

precursors, like reduced toxicity and lower processing temperatures and costs. Since metal 2-ethylhexanoates are available for a wide number of elements, are inexpensive, air-stable, and nontoxic, they seem promising precursors for the synthesis of metal oxide colloids, and an investigation of the synthesis of SnO_2 and ZnO colloids from such precursors was carried out as a case study. The successful processing of tin(II) and zinc(II) 2-ethylhexanoate for obtaining soluble, highly crystalline SnO_2 and ZnO colloids at a relatively low temperature is reported in this work. In particular, the nonhydrolytic obtainment of surface-functionalized SnO_2 nanocrystals is, to the best of our knowledge, reported for the first time. This is a specific advantage of the use of tin(II) 2-ethylhexanoate, since the number of oxygen-rich Sn precursors is extremely limited. Moreover, we report for the first time the photoluminescence properties of capped SnO_2 colloidal nanocrystals, displaying an intense blue emission.

2. Experimental Section

A. Synthesis of SnO_2 Nanocrystals. In a 500-mL three-neck flask equipped with a condenser and a thermometer, 1.25 g of tin(II) 2-ethylhexanoate ($[CH_3(CH_2)_3CH(C_2H_5)CO_2]_2Sn$) was mixed with 10 mL of diphenyl ether (DPE) and various amines, with an amine:Sn molar ratio (hereafter indicated with *r*) ranging from 0.5 to 2 for *n*-dodecylamine (DA) or kept fixed at 1 for hexylamine (HA) or octylamine (OA). The flask was thoroughly degassed with nitrogen and heated to 230 °C (for DA) or 250 °C (for HA and OA). Soon after the final temperature was reached, the liquid became yellow and was further heated for various times ranging from 5 min to 30 min when *r* varied from 2 to 0.5 in the case of DA, and for 25 min when using HA or OA. For growing larger nanocrystals, a sol was prepared with HA, and after heating at 250 °C for 25 min, a further 1.25 g of tin(II) 2-ethylhexanoate dissolved in 5 mL of DPE was injected. The temperature dropped to 230 °C after the second injection and then it arose again to 250 °C, at which temperature the flask was kept for 2 h.

The effect of the amine concentration was studied by carrying out a synthesis with hexylamine and $r = 4$, while for the effect of Sn concentration a synthesis was carried out with hexylamine, $r = 1$ and using 3.75 g of tin(II) 2-ethylhexanoate. The DPE volume was decreased with respect to the previously described syntheses in order to keep a constant total volume.

After cooling the flask, addition of methanol resulted in precipitation of the nanocrystals, which were collected by centrifugation and further purified by dispersion in hexane and subsequent recovery by addition of methanol. While the as-recovered nanocrystals are usually soluble in hexane or toluene, the solubility is lost through the purification process. In this case the nanocrystals are dispersed in hexane and a few drops of trioctylphosphine are added, and the solubility is fully recovered. The hexane−trioctylphosphine couple is the only one that provides stable suspensions. The nanocrystals functionalized with DA or, for instance, *n*-dodecanethiol, rapidly precipitate or form gel-like suspensions. Sonication of the latter helps in restoring the starting suspensions, but its stability is very low.

B. Synthesis of ZnO Nanocrystals. In a 500-mL three-neck flask equipped with a condenser and a thermometer, 0.564 g of zinc(II) 2-ethylhexanoate ($[CH_3(CH_2)_3CH(C_2H_5)CO_2]_2Zn$) was mixed with 10 mL of diphenyl ether (DPE) and dodecylamine (DA), with DA:Zn molar ratio ranging from 1 to 16. The flask was thoroughly degassed with nitrogen and heated to 250 °C for about 1 h. After cooling the flask, addition of methanol resulted in the precipitation of nanocrystals, which were soluble in hexane and stable for $r = 16$, while for $r = 8$ they could be made soluble and stable by surface exchanging with hexadecylamine and using butanol as the solvent. Finally, for $r = 2$ or 4, the nanocrystals were soluble in toluene but tended to form cloudy precipitates after several days of storage.

C. Characterization of the Nanocrystals. The structural and morphological characterization of the samples was carried out by means of transmission electron microscopy (TEM) and selected area electron diffraction (SAED). To obtain the high-resolution TEM results we used a field emission gun microscope (JEOL 2010F) that works at 200 kV and has a point to point resolution of 0.19 nm. To improve our images' contrast and resolution by avoiding the chromatic aberration inherent in HRTEM micrographs, we obtained the images by filtering the electron zero loss peak, using a Gatan image filter (GIF). Low-magnification images, as well as SAED patterns were obtained in a Philips CM30 LaB_6 microscope operated at 300 kV. SAED intensity profiles where quantified by using process diffraction software.[11]

The optical absorption curves of diluted suspensions of the nanocrystals were measured on a Shimadzu UV-2101 PC spectrophotometer with a working range from 190 to 800 nm. The photoluminesce curves were obtained by exciting the diluted samples with a He−Cd laser (17 mW on the sample). The detection set is composed of a 0.6m monochromator and a GaAs photomultiplier. To minimize noise effects, the standard chopper lock-in technique was used.

3. Results and Discussion

3.1. SnO_2 Colloids. After reaching 230 °C, the reaction mixture containing DA went from colorless to yellow and was heated for a time that decreased with increasing DA concentration. This choice was dictated by the observation that prolonged heating resulted in the sudden formation of a black-brown product, containing nanocrystalline SnO_2 and other unidentified phases. This phenomenon was delayed with decreasing the DA concentration. On the other hand, a synthesis without DA resulted again in a black-brown powder. It was supposed that DA resulted in a "clean" decomposition of the precursor, but that prolonged heating could decompose DA itself or the products of the first decomposition. Moreover, a synthesis with trioctylphosphine (TOP) instead of DA did not result in such an effect, thus it was concluded that it was peculiar of DA. Since the nanocrystals' yield when using TOP was very low, DA was finally chosen in the synthesis, and the heating times were carefully tuned in order to avoid any further decomposition of the products. Recently, in the formation of nanocrystalline oxides from the reaction of metal acetylacetonates with benzylamine, the solvolysis of the acetylacetonato ligand by the amine was proposed as the basis of the reaction mechanism.[12] The reaction mechanism leading to the formation of nanocrystals in our system is not known, but even though both amine and carbonyl centers are present, as in ref 12, it is likely that a different mechanism should be invoked. This hypothesis is suggested by several features of the present system: the different structure of the 2-ethyl-

(11) Lábár, J. L. *Proc. EUREM 12* **2000**, *III*, I379.
(12) Pinna, N.; Garnweitner, G.; Antonietti, M.; Niederberger, M. *J. Am. Chem. Soc.* **2005**, *127*, 5608−5612.

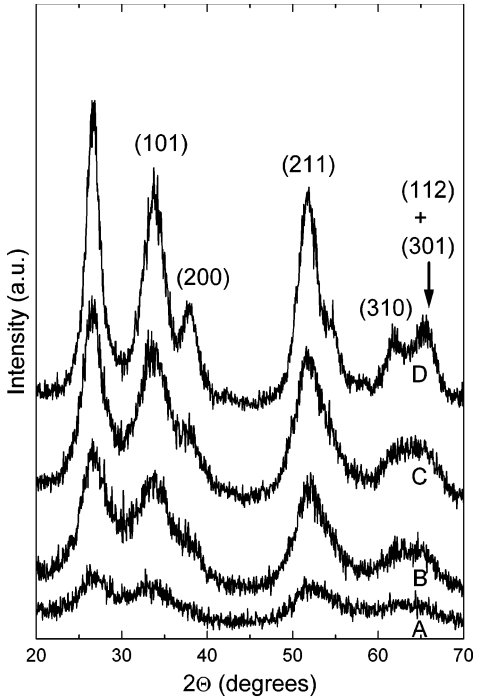

Figure 1. XRD patterns measured on dried SnO_2 nanocrystals prepared by using DA with $r = 2$ (A), HA with $r = 1$ (B), OA with $r = 1$ (C), and by multiple injection of the Sn precursor in a synthesis with HA and $r = 1$ (D). All the peaks belong to the tetragonal (cassiterite) crystallographic phase of SnO_2.

hexanoato ligands with respect to the acetylacetonato ones; the obtainment of functionalized nanocrystals, which indicates that amine is not decomposed (see also the FTIR results in Figure S1 of the Supporting Information); the use of stoichiometric amounts or small excesses of amine; and the presence of a solvent, which has a remarkable effect, as indicated by the fact that a synthesis carried out with tetradecene instead of DPE provided poorly crystalline particles.

For checking the effect of the alkyl chain length, other amines were used in the synthesis, as described in the Experimental Section. The increasing peak narrowing in the XRD patterns in Figure 1 shows that larger particles are obtained by using a shorter alkyl chain with respect to DA (curves from A to C), and this result is interpreted in terms of increasing steric hindrance to particle growth when increasing the alkyl chain length. The XRD pattern for the colloids prepared with DA refers to $r = 2$, but identical patterns were obtained for other values of r. For obtaining even larger nanocrystals, syntheses were carried out by multiple injections, as described in the Experimental Section. Curve D in Figure 1 shows that indeed larger particles can be obtained in this way, as also confirmed by HRTEM studies, but attempts to reach larger sizes by injecting larger amounts of fresh precursor failed due to the accelerated formation of carbonaceous products. Finally, higher concentrations of the tin(II) 2-ethylhexanoate or of HA did not affect the particle size, probably due also to the short processing times imposed in these cases for avoiding the formation of carbonaceous products. The large broadening of the XRD peaks does not allow a careful determination of the SnO_2 mean particle size, and HRTEM observations were

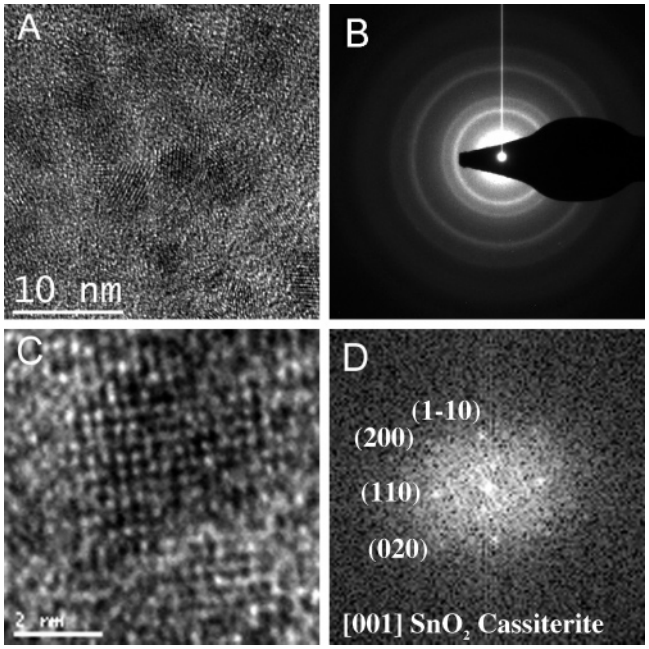

Figure 2. HRTEM image (A) and SAED (B) for the sample corresponding to curve A in Figure 1, HRTEM micrograph of a single SnO_2 nanocrystal (C), and related FFT image (D).

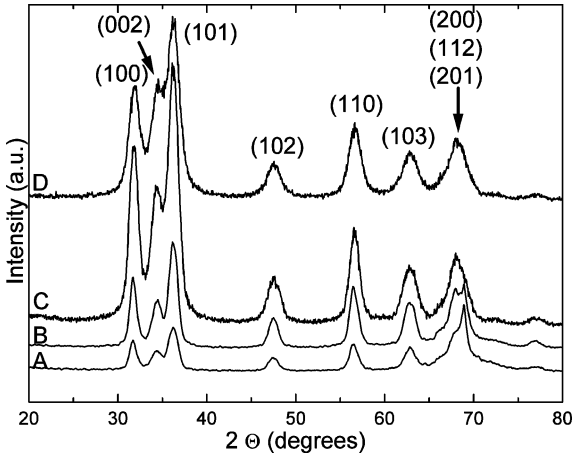

Figure 3. XRD patterns measured on dried ZnO nanocrystals prepared by using DA with $r = 2$ (A), $r = 3$ (B), $r = 8$ (C), and $r = 16$ (D). All the peaks belong to the hexagonal (zincite) crystallographic phase of ZnO.

carried out in order to elucidate the nanocrystal size. In Figure 2 the results of the TEM observations on the sample prepared with DA and $r = 2$ are reported as an example. Figure 2A shows the presence of highly crystalline nanoparticles, showing very distinct lattice fringes at close inspection. The SAED pattern in Figure 2B reveals, in agreement with the XRD patterns, the presence of only tetragonal SnO_2. The image of a single nanocrystal is shown in Figure 2C, evidencing the absence of defects in the particle, a feature that was commonly observed in the various samples.

The FFT image in Figure 3D confirms that the nanoparticle crystallized in the SnO_2 cassiterite phase. The nanocrystal was oriented along the [001] zone axis and showed the (200), (110), and (1−10) family planes. A lower magnification image of the nanocrystals is shown in Figure S2 of the Supporting Information. After carefully analyzing the HRTEM micrographs corresponding to the various samples, we found that the mean nanocrystal size corresponding to the

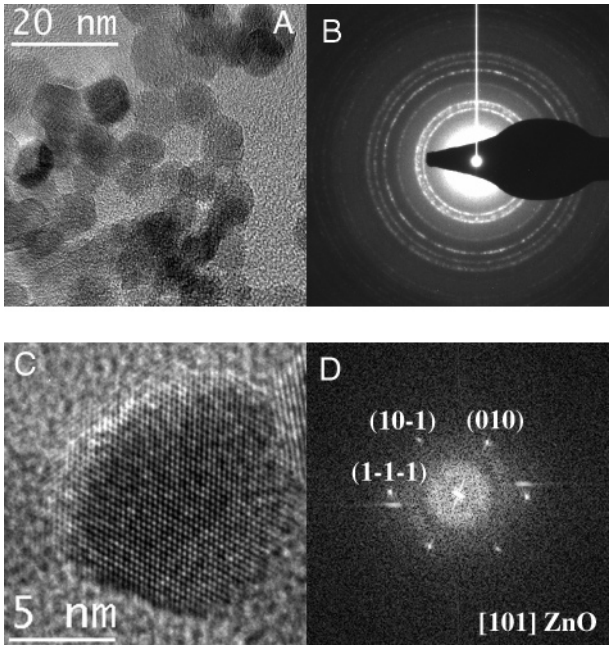

Figure 4. HRTEM image (A) and SAED (B) on ZnO nanocrystals prepared with DA and $r = 2$, HRTEM micrograph of a single ZnO nanocrystal (C), and related FFT image (D).

patterns shown in Figure 1 was about 2.5 ± 0.3 nm for curve A, 2.9 ± 0.3 nm for curve B, 3.0 ± 0.4 nm for curve C, and 3.5 ± 0.6 nm for curve D.

3.2. ZnO Colloids. The obtainment of functionalized SnO_2 nanocrystals is a valuable result by itself, since to the best of our knowledge there are very few reports about this system.[13] It seemed then interesting to check the possibility of generalizing the synthesis, and the preparation of ZnO nanocrystals was attempted by substituting tin(II) 2-ethylhexanoate with the analogous Zn precursor, as described in the Experimental Section.

The synthesis of ZnO colloids was simpler than for SnO_2. It was observed that the reaction mixture became yellow during the heating, but without any formation of carbonaceous products. In this way different DA concentrations could be used, which resulted in a tuning of the particle size, as shown by the XRD patterns in Figure 3 and TEM observations. Even for these samples, careful HRTEM studies were carried out, and in Figure 4 the results of the TEM observations on the sample related to curve A in Figure 3 are reported as an example. Figure 4A shows the presence of highly crystalline nanoparticles, with very distinct lattice fringes at close inspection. The SAED pattern in Figure 4B reveals, in agreement with the XRD patterns, the presence of only hexagonal ZnO (zincite). The image of a single nanocrystal is shown in Figure 4C, evidencing the absence of defects in the particle, a feature that was commonly observed in the various samples. The FFT image in Figure 4D confirms that the nanoparticle crystallized in the ZnO hexagonal (zincite) phase. The nanocrystal was oriented along the [101] zone axis and showed the (1−1−1), (10−1), and (010) family planes. The mean nanocrystal size derived from the HRTEM analysis on the same samples in Figure 3 was about 8.0 ± 1.0 for curve A, 7.5 ± 1.0 for curve B, 6.6 ± 0.7 nm for curve C, and 5.2 nm ± 0.6 nm for curve D.

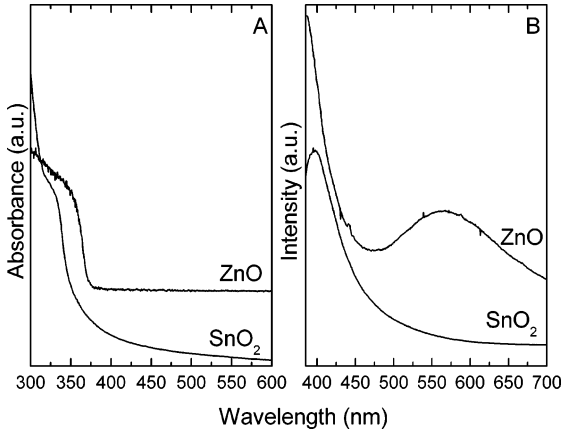

Figure 5. Optical absorption (A) and PL curves (B) measured on ZnO and SnO_2 nanocrystals. The curves have been displaced vertically for clarity.

3.3. Surface Chemistry of the Nanocrystals. As reported in the previous sections, the nanocrystal suspensions exhibit a low stability when amines are used as surface capping agents, forming cloudy precipitates that can be usually redispersed by sonication. The reversibility of the nanocrystal aggregation could indicate a weak interaction between the surface capping molecules on different nanocrystals, so we have attributed this behavior, which has already been reported for ZnO[2], to the polarization of the amine chain upon bonding with the metal cations on the nanocrystal surface. The metal surface sites indeed can be expected to display a higher charge density if compared to non-oxide semiconductors. For improving the suspension stability, it was concluded, on the basis of the previous hypothesis, that bulkier ligands could be effective, and this was the case with trioctylphospine in the case of SnO_2 or hexadecylamine in the case of ZnO.

3.4. Optical Properties of the Nanocrystals. In Figure 5 the optical absorption and the photoluminescence curves measured on a ZnO suspension are reported (synthesis parameters as in curve D of Figure 3). Similar optical absorption curves were measured for the various prepared samples, and a broad excitonic band was observed at about 350 nm. It was not possible to observe a clear shift of the peak as a function of the nanocrystal size, due to the not monodisperse size distribution and the relatively large size of the nanocrystals prepared. The photoluminescence curve displays an emission below 400 nm, which we attribute to the band-edge recombination, in agreement with other works.[7a,14]

The band is clearly shown in Figure S3 (Supporting Information). It is interesting to observe that a broad band at about 560 nm, commonly attributed to emission mediated by oxygen vacancies or other defects,[2,7a,14] is much weaker

(13) De Monredon, S.; Cellot, A.; Ribot, F.; Sanchez, C.; Armelao, L.; Gueneau, L.; Delattre, L. *J. Mater. Chem.* **2002**, *12*, 2396−2400.

(14) (a) Monticone, S.; Tufeu, R.; Kanaev, A. V. *J. Phys. Chem B.* **1998**, 102, 2854−2862. (b) Van Dijken, A.; A. Meulenkamp, E.; Vanmaekelbergh, D.; Meijerink, A. *J. Phys. Chem B.* **2000**, *104*, 4355−4360. (c) Guo, L.; Yang, S.; Yang, C.; Yu, P.; Wang, J.; Ge, W.; Womg, G. K. L. *Chem. Mater.* **2000**, *12*, 2268−2274. (d) Gu, Y.; Kuskovsky, Y. L.; Yin, M.; O'Brien, S.; Neumark, G. F. *Appl. Phys. Lett.* **2004**, *85*, 3833−3835. (e) Xiong, H.-M.; Liu, D.-P.; Xia, Y.-Y.; Chen, J.-S. *Chem. Mater.* **2005**, *17*, 3062−3064.

than the first band. Until a detailed knowledge of the reaction mechanism will be reached, we can only speculate that a possible reason could be the stoichiometric excess of oyxgen in the synthesis due to the presence of two oxygen atoms in the Zn precursor, which is double the required ZnO stoichiometry. This would limit the oxygen vacancies. This interpretation would be in agreement with recent results[8d] concerning the importance of surface reconstruction in improving the PL properties of nanocrystals.

While there are already many reports about the optical properties of ZnO nanocrystals, no reports are known about those of capped SnO_2 colloidal nanocrystals, to the best of our knowledge. The optical absorption and the PL curves measured on a SnO_2 suspension prepared with hexylamine surface-exchanged with TOP are also reported in Figure 5. In SnO_2 nanorods[15a] or nanostructures prepared by evaporation techniques,[15b−e] emission bands are reported from 500 to 600 nm, attributed to defect-mediated emission, and in uncapped SnO_2 nanoparticles a blue emission has been reported,[16] attributed to recombination of electrons in the conduction band with deep doubly ionized oxygen vacancies. In our samples, the structure of both the optical absorption and of the PL curves are similar to those of ZnO, with a blue luminescence also seen by the naked eye in diluted samples, but it is remarkable that no emission at longer wavelengths is observed, differently from ZnO. Since this is an indication that more shallow defects are absent, we attribute the peak in the optical absorption curve to exciton formation and the PL band at least partially to band-edge emission from the SnO_2 nanocrystals.

(15) (a) Cheng, B.; Russell, J. M.; Shi, W.; Zhang, L.; Samulski, E. T. *J. Am. Chem. Soc.* **2004**, *126*, 5972−5973. (b) Hu, J.; Bando, Y.; Golberg, D. *Chem. Phys. Lett.* **2003**, *372*, 758−762. (c) Hu, J.; Bando, Y.; Liu, Q.; Golberg, D. *Adv. Funct. Mater.* **2003**, *13*, 493−496. (d) Cai, D.; Chen, Y.; Jiang, J.; He, Z.; Chen, L. *Mater. Lett.* **2005**, *59*, 1984−1988. (e) Hu, J. Q.; Ma, X. L.; Shang, N. G.; Xie, Z. YX.; Wong, N. B.; Lee, C. S.; Lee, S. T. *J. Phys. Chem. B.* **2002**, 106, 3823−3826.

(16) Gu, F.; Wang, S. F.; Lü, M. K.; Zhou, G. J.; Xu, D.; Yuan, D. R. *J. Phys. Chem. B.* **2004**, 108, 8119−8123.

Conclusions

In conclusion, the successful preparation of soluble SnO_2 and ZnO nanocrystals has shown the possibility of using metal 2-ethylhexanoates as a new class of precursors. While the preparation of ZnO nanocrystals is well-known from many other procedures, we have introduced tin(II) 2-ethylhexanoate as a unique, convenient precursor for a simple synthesis of capped SnO_2 nanocrystals. The luminescence properties of the ZnO nanocrystals resemble those already reported, but for the first time a blue emission is reported from capped SnO_2 nanocrystals. The preparation of larger nanocrystals and the eventual shape control are an open problematic arising from this work, together with a detailed study of the decomposition mechanism of the precursor, necessary in view of an efficient use of other 2-ethylhexanoates for obtaining different oxides.

Acknowledgment. The authors thank the XRD and FTIR units of the Serveis Científico-Tècnics of the University of Barcelona for their cooperation. Mauro Epifani acknowledges the financial support from the National Council of Research (CNR) for a short-term mobility at the University of Barcelona (Spain). This work was supported by the European Union in the frame of the NANOS4 (Grant NMP4-CT-2003-001528) project.

Note Added after ASAP Publication. The Supporting Information file published ASAP November 12, 2005, was incorrect; the corrected version was published November 15, 2005.

Supporting Information Available: FTIR curve measured on dried SnO_2 colloids prepared with hexylamine low magnification image of SnO_2 nanocrystals, PL curves on diluted suspensions. This material is available free of charge via the Internet at http://pubs.acs.org.

CM051642U